NDACC UV/Vis Algorithm Theoretical Background Document (ATBD)

Version 1.0: March 2020

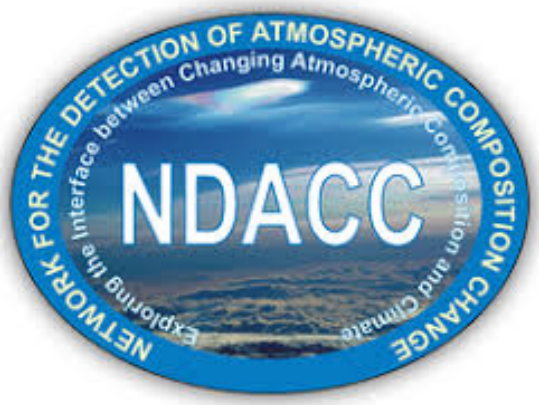

Editors:

Michel Van Roozendael (NDACC UV-Vis working group co-chair)
Karin Kreher (NDACC UV-Vis working group co-chair)

Contributing authors:

François Hendrick (BIRA-IASB) (Main author)
Michel Van Roozendael (BIRA-IASB)
Steffen Beirle (MPIC)
Caroline Fayt (BIRA-IASB)
Udo Frieß (UHeid)
Martina M. Friedrich (BIRA-IASB)
Karin Kreher (BK Scientific)
Andreas Richter (IUP-Bremen)
Thomas Wagner (MPIC)

Contents

1 Introduction

This document describes the approaches and methods in use within NDACC for the retrieval of ground-based UV-Vis Differential Optical Absorption Spectroscopy (DOAS) data products. One usually distinguishes between zenith-sky twilight stratospheric measurements (such as ozone and nitrogen dioxide column measurements conducted within NDACC for several decades) and Multi-AXis DOAS (MAX-DOAS) measurements of the tropospheric composition.

In recent years, NDACC and NDACC-related stations equipped with MAX-DOAS instruments have grown in number with a potential to deliver harmonised and quality-assessed tropospheric data products for use in operational satellite validation programme or in support of atmospheric monitoring services such as CAMS (Copernicus Atmospheric Monitoring Service) or C3S (Copernicus Climate Change Service). In view of this evolution, the UV-Vis working group has supported the development and integration in NDACC of a number of new MAX-DOAS data products addressing the monitoring of several key tropospheric species, in particular NO2, HCHO and aerosols. This process involved the assessment of MAX-DOAS instrumental performance in various intercomparison field campaigns (CINDI, Roscoe et al., 2010; MADCAT, http://joseba.mpch-mainz.mpg.de/mad_cat.htm, and CINDI-2, Kreher et al., 2019) as well as the optimisation and harmonisation of retrieval methods, in particular within the recent ESA FRM$_4$DOAS project (Fiducial Reference Measurements from Ground-based DOAS Air-Quality Observations; see http://frm4doas.aeronomie.be/).

This document describes the algorithms and methods used to retrieve the current NDACC UV-Vis data products, namely:

- total ozone (O_3) vertical columns
- total stratospheric columns and vertical profiles of nitrogen dioxide (NO_2)
- total vertical columns and profiles of bromine monoxide (BrO)
- lower tropospheric aerosol extinction profiles based on MAX-DOAS O_4 measurements
- lower tropospheric gas vertical profiles of NO_2 and HCHO based on MAX-DOAS measurements

It is structured as follows: The main principles of the ground-based DOAS technique are described in Section 2, while Sections 3 and 4 concentrate on methods specific to zenith-sky and MAX-DOAS retrievals, respectively. Section 5 introduces the methods used for the calculation of uncertainties. The characterisation of the vertical and horizontal smoothing effects is the subject of Sections 6 and 7. Section 8 briefly addresses the impact of clouds and conclusions are given in Section 9.

2 Principle of the DOAS method

The determination of the abundance of atmospheric trace gases using the DOAS method is based on a two-step approach (Platt and Stutz, 2008; see also Hönninger et al., 2004). In the first step, which involves a spectral fitting procedure based on the Beer-Lambert extinction law, high frequency trace gas absorption features are quantified against known laboratory absorption cross-sections. The end product is the so-called differential slant column density (DSCD), which represents the difference

between the trace-gas concentration integrated along the effective light path in the current spectrum and in a reference spectrum. In the second step, resulting DSCDs are converted into vertical column densities (VCDs) or vertical profiles, using radiative transfer calculations performed at one wavelength representative of the fitting interval.

In DOAS, the atmospheric model is the Beer-Lambert extinction law for trace gas absorbers, that describes the relationship between the incident light intensity at the location of the light source (or, in case of scattered light, at the top of the atmosphere) and the transmitted intensity at the location of the instrument detector:

$$I(\lambda) = I_0(\lambda)\exp(-\int_0^L \left[\sum_i \sigma_{a,i}(\lambda)n_i + \sigma_R(\lambda)n_R + k_M(\lambda)\right] ds) \quad (1)$$

where $I_0(\lambda)$ and $I(\lambda)$ are the incident and transmitted intensity, respectively, at wavelength λ, L is the length of the effective light path, $\sigma_{a,i}(\lambda)$ and n_i are the absorption cross section at wavelength λ and number density of the absorber i, respectively, $\sigma_R(\lambda)$ is the Rayleigh scattering cross section at wavelength λ, n_R is the air density, $k_M(\lambda)$ is the Mie extinction coefficient at wavelength λ, and ds is the thickness of the atmospheric layer traversed by the light.

The optical depth $\tau(\lambda)$ can be introduced

$$\tau(\lambda) = -ln\left[\frac{I(\lambda)}{I_0(\lambda)}\right] = \sum_i(\int_0^L \sigma_{a,i}(\lambda)n_i ds) + \int_0^L \sigma_R(\lambda)n_R ds + \int_0^L k_M(\lambda) ds \quad (2)$$

and Eq. (1) becomes

$$\tau(\lambda) = \sum_i(\int_0^L \sigma_{a,i}(\lambda)n_i ds) + \tau_R(\lambda) + \tau_M(\lambda) \quad (3)$$

where $\tau_R(\lambda)$ and $\tau_M(\lambda)$ are the Rayleigh and Mie scattering optical depths, respectively.

Assuming that the height dependency of the absorption cross sections $\sigma_{a,i}(\lambda)$ can be neglected, i.e. absorption cross-sections are weakly dependent on the temperature and pressure along the effective light path, the summation and the integral in Eq. (3) can be exchanged and $\tau(\lambda)$ can be expressed as:

$$\tau(\lambda) = \sum_i \sigma_{a,i}(\lambda)\, SCD_i + \tau_{MR}(\lambda) + \tau_M(\lambda) \text{ with } SCD_i = \int_0^L n_i ds \quad (4)$$

SCD_i is the so-called slant column density of the absorber i and is the direct product of the DOAS analysis. It represents the total amount of the absorber i per unit area integrated along the effective light path.

At this point, the so-called DOAS concept is introduced into the derivation. It is based on the fact that Rayleigh and Mie scattering vary weakly with wavelength, while the molecular absorption cross section $\sigma_{a,i}(\lambda)$ of a certain species can be separated into a low and a high frequency component or a broad-band and a differential absorption cross section $\sigma^S_{a,i}(\lambda)$ and $\sigma'_{a,i}(\lambda)$, respectively:

$$\sigma_{a,i}(\lambda) = \sigma'_{a,i}(\lambda) + \sigma^S_{a,i}(\lambda) \quad (5)$$

By replacing $\sigma_{a,i}(\lambda)$ by (5) in Eq. (4) and by substituting components with low frequency variations ($\sigma^{S}_{a,i}(\lambda)$, Rayleigh and Mie scattering), which follow simple power laws, by a polynomial $P = \sum_P a_P \lambda^P$, the DOAS equation is then obtained:

$$\tau(\lambda) = -ln\left[\frac{I(\lambda)}{I_0(\lambda)}\right] = \sum_i \sigma'_{a,i}(\lambda)\, SCD_i + \sum_P a_P \lambda^P \quad (6)$$

Knowing the reference spectrum $I_0(\lambda)$, the slant column densities SCD_i and coefficient a_p can be retrieved by adjusting the differential absorption cross sections $\sigma'_{a,i}(\lambda)$ (determined from laboratory measurements) to the measured optical depth by means of a linear least squares fit.

For ground-based observations, it is a common method to use a measured spectrum $I'_0(\lambda)$ with the smallest absorptions as reference spectrum, since it is not possible, in contrast to satellite measurements, to record an extraterrestrial solar spectrum with the same instrument. For all viewing directions of the MAX-DOAS measurements, the zenith spectrum of the scan is usually chosen as reference. In the case of the zenith-sky twilight observations, a daily noon zenith spectrum is used.

According to this, Eq. (6) can be rewritten as:

$$\tau(\lambda) = -ln\left[\frac{I(\lambda)}{I'_0(\lambda)}\right] = \sum_i \sigma'_{a,i}(\lambda)\,(SCD_i - SCD_i^{ref}) + \sum_P a_P \lambda^P \quad (7)$$

where $(SCD_i - SCD_i^{ref}) = DSCD_i$ are the so-called differential slant column densities of the absorber *i*. The absorber amount in the reference spectrum is usually determined by an extrapolation method (e.g. a Langley-plot analysis) and added to the retrieved $DSCD_i$ to obtain absolute slant column densities SCD_i.

3 Zenith-sky twilight stratospheric measurements

Measurements of the sunlight scattered at zenith during morning and evening twilight have been used for several decades to derive the abundance of several stratospheric species, in particular ozone (O_3), nitrogen dioxide (NO_2), bromine monoxide (BrO), and chlorine dioxide (OClO). Methods were designed in the late eighties and are described in several papers, e.g. Pommereau and Goutail, 1988; Solomon et al., 1989; McKenzie et al., 1991; Fiedler et al., 1993; Kreher et al., 1997; Richter et al., 1999; Van Roozendael et al., 1994 and 1998; Struthers et al., 2004; Hendrick et al., 2008. This technique exploits the particular geometry of the solar light penetration in the atmosphere during twilight to enhance the sensitivity towards stratospheric absorbers. Below, we briefly describe the principle used to derive total columns of O_3 and NO_2, as well as vertical profiles of NO_2 and BrO.

3.1 Total O_3 and stratospheric NO_2 vertical columns

Total O_3 VCDs are retrieved from twilight zenith-sky UV-Vis observations using the following expression (see e.g. Hendrick et al., 2011):

$$VCD(\theta) = \frac{DSCD(\theta) + RCD}{AMF(\theta)} \quad (8)$$

where *VCD(θ)* is the O_3 VCD at the effective SZA *θ*, *DSCD(θ)* is the O_3 DSCD at SZA *θ*, *RCD* is the residual O_3 amount in the reference measurement (generally a fixed spectrum usually recorded at high sun around local noon), and *AMF(θ)* is the AMF at SZA *θ*.

Given expression (8), the retrieval of vertical columns consists of four steps: (1) slant column spectral fitting, (2) determination of residual amount in the reference spectrum, (3) conversion of absolute slant columns into vertical columns using appropriate AMFs, and (4) averaging of the vertical columns over a limited SZA range around 90° SZA. Regarding step (2), *RCD* is derived using the so-called Langley plot method, which consists in rearranging Eq. (8) and plotting *DSCD(θ)* as a function of *AMF(θ)*, the intercept at AMF = 0 giving *RCD* (Roscoe et al., 1994; Vaughan et al., 1997). *VCD(θ)* is then derived in step (3) by dividing the absolute O_3 SCD at SZA θ (*DSCD(θ)*+*RCD*) by an appropriate *AMF(θ)*. Regarding step (4), sunrise and sunset O_3 column data are derived by averaging VCDs estimated with Eq. (8) over a limited SZA range around 90°SZA.

The NDACC UV-Vis WG has released recommendations and provided corresponding settings for each of those four steps. Those can be found at http://ndacc-uvvis-wg.aeronomie.be/tools.php. In brief, the recommended standard NDACC O_3 AMF climatology (see Hendrick et al., 2011) is based on the TOMS version 8 (TV8) ozone and temperature profile climatology (Barthia et al., 2004). It consists of 18 look-up tables (LUTs) generated using the UVSPEC/DISORT RTM (Mayer and Kylling, 2005) initialised with TV8, each of these LUT corresponding to one TV8 latitude (10° latitude bands between 90°S and 90°N). The other entry parameters are: wavelength, ground albedo, altitude of the station, day of the year, and SZA. The extraction of appropriate O_3 AMFs at a given station is done by using the dedicated interpolation routine in Fortran developed in the framework of the NDACC UV-Vis WG. Regarding the selection of the SZA range representative of twilight conditions, the best compromise between accuracy and precision is achieved in the 86-91° SZA range. The recommended NDACC approach is to apply a linear fit to the VCDs in the above SZA range and then derive the column value at an effective SZA, which is usually fixed at 90°.

Within the NDACC UV-Vis WG, the same 4-step approach is applied for the retrieval of stratospheric NO_2 VCDs (see e.g. Van Roozendael et al., 1994). As for O_3, the corresponding NDACC recommendations are available at http://ndacc-uvvis-wg.aeronomie.be/tools.php. Recommended sunrise and sunset NO_2 AMF LUTS have been generated using the harmonic climatology of stratospheric NO_2 profiles developed by Lambert et al. (1999, 2000), complemented between 12 and 17 km altitude by a climatology derived from SAOZ balloon profile observations.

3.2 Stratospheric NO_2 and BrO vertical profiles

In addition to the standard NDACC approach providing VCDs, stratospheric NO_2 but also BrO vertical profiles can be retrieved from zenith-sky twilight observations. The inversion is based on the dependence of the mean scattering height with SZA: during twilight, as the SZA increases, the mean scattering height rises into the absorber layer, so each slant column measurement is mainly representative of the absorber concentration in a given altitude range. Thus, the observed slant column variation during twilight depends on the vertical distribution of the trace gas and the latter can be retrieved by applying the linear OEM approach (see Preston et al., 1997; Hendrick et al., 2004 and 2008). The measurement vector *y* consists in a set of measured twilight (sunrise or sunset) NO_2 or BrO DSCDs usually obtained in the 75-94°SZA range.

In the case of NO_2 and BrO, the simple geometric dependence on which the profiling approach is based, is complicated by the rapid variation of their concentrations with local SZA at twilight due to photochemistry (see Figure 1). In order to calculate appropriate weighting functions (WFs), it is therefore important to use a RTM that accounts for the two-dimensional (2D: altitude, SZA) photochemical variation of NO_2 and BrO, at least for the incident beam (first order approximation). The 2D NO_2 and BrO concentration fields are generally taken from stacked box photochemical model simulations initialized with 3D-CTM meteorological and chemical fields extracted at the location of the station (see e.g. Hendrick et al., 2004 and 2008).

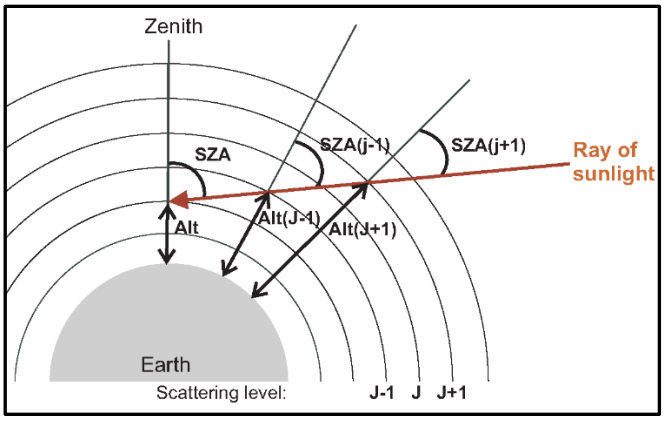

Figure 1: **Variation of the local SZA along the path of a given ray. SZA(j)=local SZA of the ray in the j^{th} scatter level.**

4 MAX-DOAS tropospheric measurements

The MAX-DOAS technique was developed in the early 2000's as an extension of the zenith-sky DOAS technique to monitor lower tropospheric species such as NO_2, formaldehyde (HCHO), sulphur dioxide (SO_2), nitrous acid (HONO), glyoxal (CHOCHO), BrO, as well as aerosols. MAX-DOAS spectrometers measure the absorption of sunlight scattered by molecules at a series of elevation angles from the horizon to the zenith (see Figure 2), thereby increasing the sensitivity of the measurements to absorbers present close to the ground.

Lower tropospheric aerosol extinction and trace gas vertical profiles are retrieved for each MAX-DOAS scan by applying a profiling algorithm to the corresponding sets of DSCDs measured at the different elevation angles. The zenith spectrum of the scan is usually chosen as reference, in this way also removing the contribution of the stratosphere in off-axis DSCDs, which can be significant for a species like NO_2. The MAX-DOAS profiling technique is based on the fact that the mean scattering height rises into the atmosphere with the increase of the elevation angle and probes the layers where the tropospheric absorber is present. So, each measured DSCD of a MAX-DOAS scan is representative of the absorber concentration in a given altitude range and therefore the observed DSCD variation as a function of the elevation angle depends on the vertical distribution of the absorber.

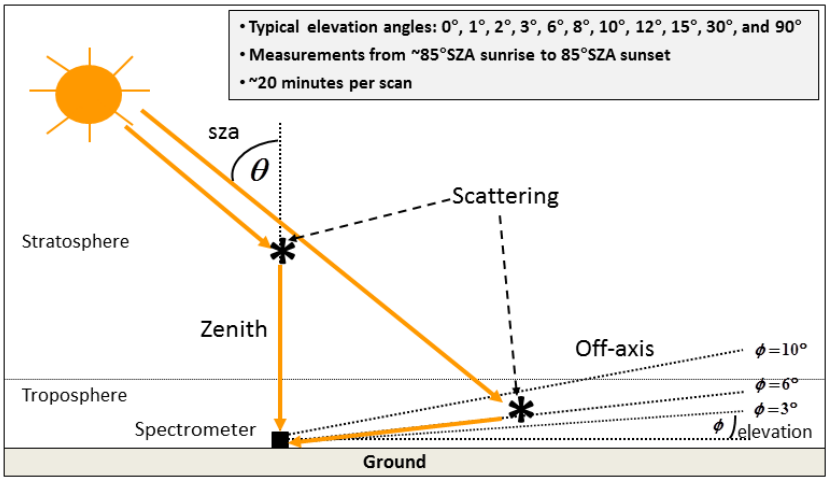

Figure 2: **Sketch illustrating the MAX-DOAS viewing geometries (off-axis and zenith). Typical elevation angle values used during a scan are given in the top right grey frame**.

The two main different MAX-DOAS profiling approaches that currently exist are the following: the Optimal Estimation Method (OEM) that gives vertical distributions of aerosol and trace gas on a defined altitude grid (e.g. 0 to 4 km in 200m steps) and the parameterized retrieval scheme that gives a first order description of typical vertical distributions (see Figure 3).

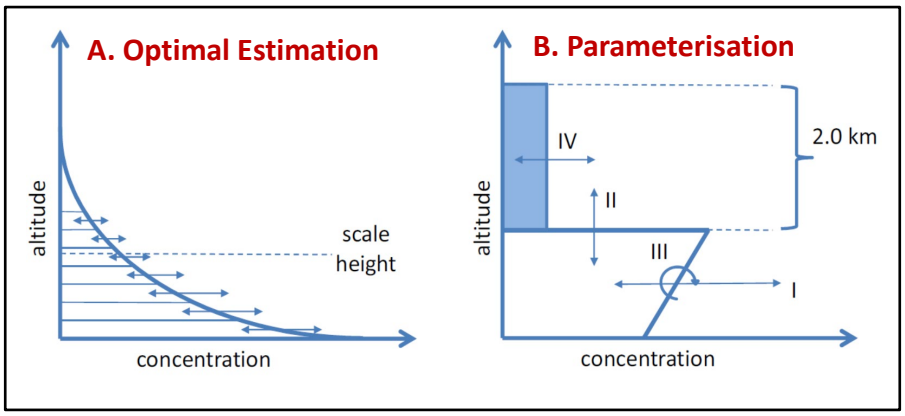

Figure 3: **Schematic of profile parameterizations used in the OEM (A/left) and parametrized (B/right) approaches. In the case of method B, only a limited number of parameters are retrieved, e. g. (I) tropospheric VCD or AOD, (II) mixing layer top height, (III) shape parameter, (IV) free tropospheric VCD. Adapted from Vlemmix et al. (2015).**

Both methods use a two-step procedure. First, the aerosol extinction vertical profiles are retrieved for each MAX-DOAS scan from the corresponding measured oxygen collisional dimer O_4 DSCDs. The principle of this retrieval is the following: since the O_4 vertical profile is well-known and nearly constant (it varies with the square of the O_2 concentration), O_4 DSCD measurements can provide information on the vertical distribution of aerosols (Wagner et al., 2004; Frieß et al., 2006). This first step is required since the light path length through the atmosphere (and thus the measured trace gas DSCD) strongly depends on the aerosols and therefore a good estimate of the vertical distribution of the aerosols is needed to calculate appropriate trace gas weighting functions (WFs) or SCDs. In the second step, the

OEM-based or parameterized method is applied to the measured trace gas DSCDs in order to retrieve vertical profiles.

In the OEM formalism (see Rodgers, 2000), a profile x is retrieved given an a priori profile x_a, the measurements y (DSCDs as a function of scan elevations for tropospheric trace gas profiles), their respective uncertainty covariance matrices (S_a and S_ε, respectively), and the matrix K of the WFs that indicate the sensitivity of the differential slant column abundances at each SZA to a change in the vertical profile:

$$x = x_a + S_a K^T (K S_a K^T + S_\varepsilon)^{-1} (y - K x_a) \text{ with } K = \frac{\partial y}{\partial x} \text{ and } K^T \text{ is the transpose of } K \quad (9)$$

The weighting functions have been determined by consecutively perturbing each layer of the a priori profile and recalculating the set of measurements using a radiative transfer model (RTM) as forward model. The OEM for a linear case is considered for optically thin absorbers like NO_2 and HCHO because measured DSCDs depend linearly on the concentrations in each profile layer. Therefore, the WF matrix K is independent of the state (Heskes and Boersma, 2003) and a single inversion step is sufficient. In case of strong absorbers like O_4, a non-linear iterative approach based on a Gauss-Newton or Levenberg-Marquart minimisation scheme must be used (Rodgers, 2000; see also Frieß et al., 2006; Clémer et al., 2010; Friedrich et al., 2019):

$$x_{i+1} = x_i + (S_a^{-1} + K_i^T S_\varepsilon^{-1} K_i)^{-1} [K_i^T S_\varepsilon^{-1} \big(y - F(x_i)\big) - S_a^{-1} (x_i - x_a)] \quad (10)$$

where F is the forward model operator, K_i is the sequentially updated WF at step i, and the superscripts T and -1 denote the transposed and inversed matrix, respectively.

The a priori profile x_a and the covariance matrices of uncertainties in the a priori profile and in the measurements (S_a and S_ε, respectively) are key parameters for the retrieval. Because the inversion problem is ill-posed (there are more elements in the state vector x than independently measured elements in the vector y and therefore no unique solution to Eq. 9 and 10), a priori constraints are necessary to reject unrealistic solutions that might be consistent with the measurements. A priori profiles can be built by imposing a profile shape (e.g. exponential-decreasing) or taken from the output of a 3D Chemistry-Transport model (CTM).

Since the residuals from the DOAS fitting are in most cases dominated by the random noise of the detector, the measurement covariance matrix S_ε is chosen diagonal with values corresponding to the statistical errors on the trace gas DOAS fitting. The S_ε matrix being fixed, the a priori covariance matrix S_a can act like a tuning parameter (see e.g. Schofield et al., 2004). The selected variance value should maximize the information content without leading to undesired oscillations in the retrieved profiles. S_a also contains extra-diagonal terms in order to account for correlations between trace gas concentrations at different altitude levels. These terms are usually added as Gaussian functions as follows (Barret et al., 2002):

$$S_{a\,ij} = \sqrt{S_{a\,ii} S_{a\,jj}} e^{-\ln(2)\left(\frac{z_i - z_j}{\gamma}\right)^2} \quad (11)$$

where z_i and z_j are the altitudes of i^{th} and j^{th} levels, respectively, and γ is the HWHM (half of the correlation length). In the case of MAX-DOAS retrievals, the correlation length usually varies between 50 and 200m.

In contrast to the OEM, the parameterized approach makes use of a profile shape parameterization with just a few free parameters (e.g. layer height, column amount, shape parameter; see Figure 3). These are retrieved by combining off-line forward simulations of AMFs and SCDs and a least-square minimisation strategy (see e.g. Li et al., 2010; Wagner et al., 2011; Vlemmix et al., 2010, 2011, and 2015; Beirle et al., 2019). The main reason to use a low number of free parameters is that the information content of MAX-DOAS observations with respect to the vertical distribution of aerosols and trace gases is limited, and therefore, a sufficiently wide range of possible profile shapes can be retrieved with a limited but appropriate choice of free parameters (Vlemmix et al., 2015).

Regarding the minimization strategy, standard least-square methods like Levenberg-Marquart can be used (see e.g. Li et al., 2010) or faster approaches which do not required the calculation of derivatives, like the simplex (see Vlemmix et al., 2011) or Monte Carlo (see Beirle et al., 2019) methods.

A description of the OEM-based and parameterized algorithms and their corresponding forward models currently used in the MAX-DOAS community can be found in Frieß et al. (2019), Hendrick et al. (2006) and Wagner et al. (2007).

5 Error analysis

In this section, an overview on the error analysis methods used for the different NDACC UV-Vis data products is given. The uncertainties associated to the DOAS spectral fit are not described here.

5.1 Total O_3 and stratospheric NO_2 columns

The error budget of total O_3 columns is obtained by considering error sources affecting the determination of the DSCD, RCD, and AMF (see Eq. 8). These error sources are summarized below, based on Hendrick et al. (2011):

- Uncertainties associated to the least-squares DOAS spectral fit are due to detector noise, instrumental imperfections (small wavelength scale and resolution changes, etaloning and non-linearities of the detector, stray-light, polarisation effects, etc) as well as uncertainties or unknowns in the signal modelling (Ring effect, unknown absorbers, wavelength dependence of the AMF, etc). To some extent, such uncertainties are pseudo-random in nature and, as such, can be estimated statistically from the least-squares fit procedure. These random uncertainty sources should be added up to systematic uncertainties on ozone absorption cross sections in the Chappuis bands and on their limited temperature dependence.
- The uncertainty on the determination of residual amount in the reference spectrum is limited by the method used to derive the O_3 VCD at the time of the reference spectrum acquisition (here Langley-plot approach).
- The uncertainties of O_3 AMF are considered as pseudo-random and originate mainly from the type of radiative transfer model used for AMF calculation and the corresponding input settings: selected O_3 vertical profile climatology, clouds and stratospheric aerosol load scenarios, and surface albedo.

Similar error sources also apply for the retrieval of stratospheric NO_2 VCDs based on the standard NDACC AMF-based approach (see Van Roozendael et al., 1998).

5.2 Tropospheric and stratospheric products derived by OEM

In the OEM, the total error of the retrieved profile is the sum of three errors (Rodgers, 2000): the error due to the smoothing of the true profile or smoothing error, the error due to random and systematic errors in the measurements, and the error due to systematic errors in the forward model.

The smoothing error covariance matrix S_s can be calculated using the following expression (Rodgers, 2000):

$$S_s = (A - I)\, S_x\, (A - I)^T \tag{12}$$

where S_x is a realistic covariance matrix of the true profile, A is the averaging kernels matrix and I is the identity matrix. S_x also contains extra-diagonal terms in order to account for correlations between trace gas concentration values at different altitude levels. In a first approximation, the S_x matrix is generally chosen identical to S_a.

The retrieval noise S_m which is the retrieval error covariance resulting from measurement error is defined as (Rodgers, 2000):

$$S_m = G\, S_\varepsilon\, G^T \text{ with } G = \frac{\partial \hat{x}}{\partial y} = S_a K^T (K S_a K^T + S_\varepsilon)^{-1} \tag{13}$$

where S_ε is the measurement error covariance matrix, and G is the contribution functions matrix expressing the sensitivity of the retrieved profile to changes in the measured trace gas slant column abundances. As already mentioned, the S_ε matrix was chosen diagonal with values corresponding to the statistical errors on the DOAS fitting.

The forward model parameter error S_f is the retrieval error due to errors in the forward model parameters (e.g. uncertainties related to the pressure, temperature profiles, albedo, rate constants in the photochemical model in the case of stratospheric products, etc). S_f is given by the following expression (Rodgers, 2000):

$$S_f = G\, K_b\, S_b\, K_b^T\, G^T \tag{14}$$

where G is the contribution functions matrix (see Eq. 13), K_b is the sensitivity of the forward model to perturbations of forward model parameters b, and S_b is the covariance matrix of b. S_f cannot be determined easily due to the large number of forward model parameters.

5.3 Tropospheric products derived using parameterized profiles

The main error source for the parameterized approach is the a priori assumptions made for the forward model calculations, like e.g. the profile shapes, aerosol properties, ground albedo, etc. If the chosen parameterization does not properly cover all the real scenarios occurring at a given station, it can be the source of systematic errors in the profile inversion (Beirle et al., 2019; Vlemmix et al., 2010). The estimation of the uncertainty related to the forward model parameters can be done through sensitivity studies (see e.g. Vlemmix et al., 2010).

6 Vertical averaging kernels

The sensitivity of the ground-based DOAS and MAX-DOAS measurements to the vertical distribution of trace gases is usually characterized using the averaging kernels (AKs; see Rodgers, 2000), which correspond to the rows of the averaging kernel matrix *A*. This matrix is derived using the following expression (Rodgers, 2000):

$$A = \frac{\partial \hat{x}}{\partial x} = (K^T S_\varepsilon^{-1} K + S_a^{-1})^{-1} K^T S_\varepsilon^{-1} K \quad (15)$$

AKs express the relationship between the retrieved profile $\hat{x}$ and the true atmospheric profile x through the following equation:

$$\hat{x} = x_a + A(x - x_a) + \text{Error terms} \quad (16)$$

Following Eq. (16), the retrieval of any profile point is an average of the entire true profile weighted by the row of the *A* matrix corresponding to the altitude of the retrieved profile point. For an ideal observing system, the *A* matrix would be therefore equal to the identity matrix. In the reality, the retrieved profile is only a smoothed perception of the true profile. The vertical resolution of this smoothed information at a given altitude can be estimated by taking the FWHM of the main peak of the corresponding averaging kernel. Another important characterization parameter which can be derived from the *A* matrix is the number of degrees of freedom for signal (DOFS) providing an estimate of the number of independent pieces of information that can be retrieved from the measurements. This parameter is given by the trace of *A* (Rodgers, 2000).

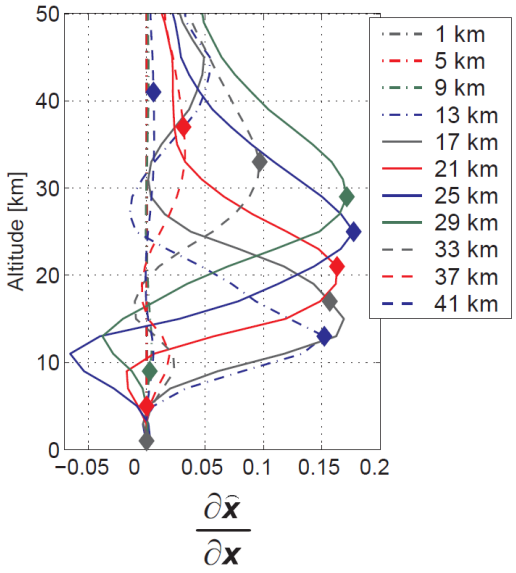

Figure 4: Typical example of AKs for stratospheric NO_2 OEM-based retrieval. Plain diamonds indicate the nominal altitude at which each averaging kernel should peak (Hendrick et al., 2004). A typical stratospheric BrO AKs plot can be found in Hendrick et al. (2009).

Figures 4 and 5 show typical examples of AKs for stratospheric NO_2 and tropospheric aerosol and trace gas OEM-based retrievals, respectively.

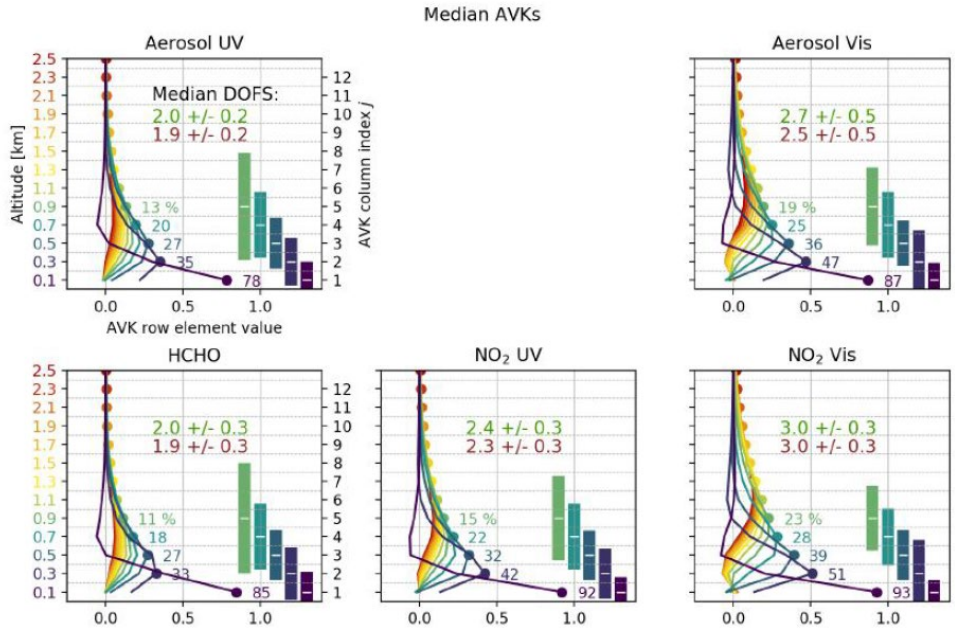

Figure 5: **Typical example of AKs for lower tropospheric OEM-based aerosol extinction and trace gas profile retrievals from CINDI-2 campaign MAX-DOAS measurements (Tirpitz et al., 2020).**

From Preston et al. (1997), Hendrick et al. (2004), and Hendrick et al. (2009), it was found that 13-37 km and 13-27 km are the altitude ranges where twilight zenith-sky measurements give significant information about the vertical distribution of NO_2 and BrO, respectively. From Figure 4, we also see that the vertical resolution is about 8 km at 13 km of altitude and reaches 20 km at an altitude of 33 km. Typical values for the trace of *A* are about 2, meaning that there are about 2 independent pieces of information in the zenith-sky twilight measurements of NO_2 and BrO.

The examination of the MAX-DOAS NO_2 AKs in Figure 5 indicates that the inversions are sensitive to the layers from the surface up to 1-1.5 km. The corresponding DOFS is about 2-3. It should be noted that AKs (and therefore the vertical sensitivity) have not been derived so far for retrievals based on the parameterized approach.

A typical example total O_3 column AK is shown in Figure 6. Since the mean scattering layer is located around 14 km altitude, the sensitivity of zenith sky twilight measurements to tropospheric ozone is limited, with averaging kernel value smaller than 0.5 below 8 km, and increases in the stratosphere where averaging kernel value is larger than 1 between 14-30 km altitude. So, the twilight zenith-sky UV-vis total column O_3 measurements are strongly weighted by the contribution of the stratosphere and therefore show very limited sensitivity to the uncertainties on parameters affecting tropospheric ozone like e.g. Mie scattering in a cloud layer. However, these measurements are sensitive to the tropospheric ozone column used for the AMF calculation which acts as a ghost column in the total column retrieval.

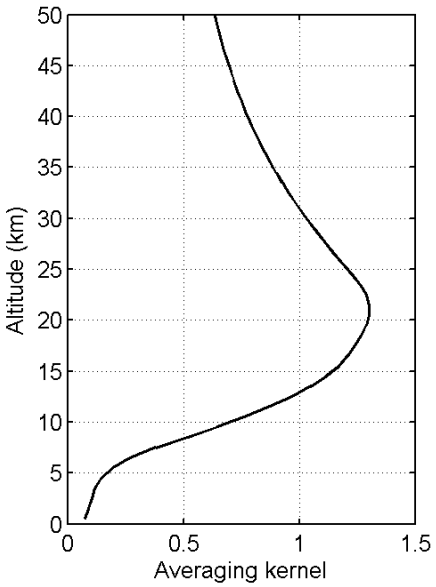

Figure 6: Column AK computed for 90°SZA in zenith-sky geometry using O_3 and temperature profiles corresponding to 45°N/325 DU in June extracted from the TV8 climatology. The wavelength is fixed to 500 nm. From Hendrick et al. (2011).

7 Horizontal smoothing

In contrast to *in-situ* observations such as an ozone monitor located at the surface, remote sensing observations average over space and time providing integrated values representative for values averaged over a certain volume. When evaluating the air volume for which these measurements are representative, quantities like vertical and horizontal resolutions of the measurements and horizontal displacement of the measured air volume are usually considered. Regarding the evaluation of the latter, simple parameterized approaches are usually used (Richter et al., 2013) and those are described below.

7.1 Zenith-sky stratospheric O_3 and NO_2 products

For zenith-sky twilight observations, the horizontal displacement of the measurement volume depends mainly on *SZA,* and the light path has in first approximation two separate parts: one from the sun to the scattering point in altitude *z* which is determined by the solar position, and a second one passing vertically through the atmosphere from altitude *z* to the instrument on the ground (Figure 7). The horizontal displacement *x* from the instrument location can be computed for each scattering height *z* by:

$$x(z,i) = (i - z).\tan(SZA) \quad (17)$$

For the effective signal, the average over the horizontal displacements for all scattering altitudes *z* needs to be calculated, weighted by the respective radiation received from this altitude at the surface *WF(z)*:

$$d(i) = \frac{\sum_{z,i=0}^{top-atmosphere} x(z,i).WF(z)}{\sum_{z,i=0}^{top-atmosphere} WF(z)} \quad (18)$$

The resulting distances *d,* calculated by using a simple ray-tracing model, are shown in Figure 8 and can be as large as 500 km in the stratosphere at twilight.

LUTs of distance *d* with *SZA* and altitude as entries can be used in combination of the azimuth solar angle to report the mean location of the effective air mass corresponding to the retrieved twilight total O_3 columns and stratospheric NO_2 profiles and columns.

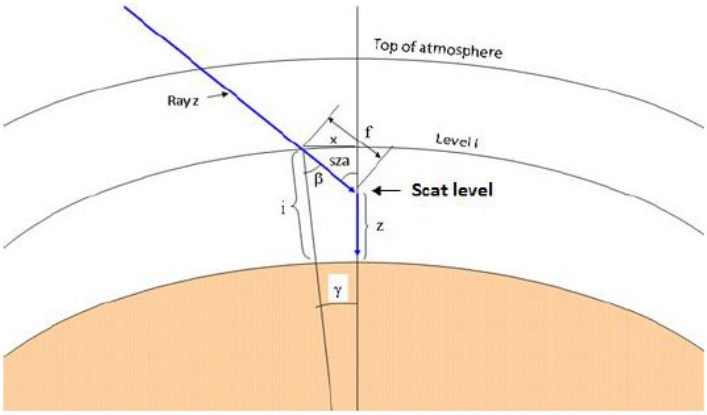

Figure 7: Sketch of the light path for zenith-sky observations. Indicated is the distance *x* that the measurement point has at altitude level *i* for a scattering altitude *z* at solar zenith angle SZA (Richter et al., 2013).

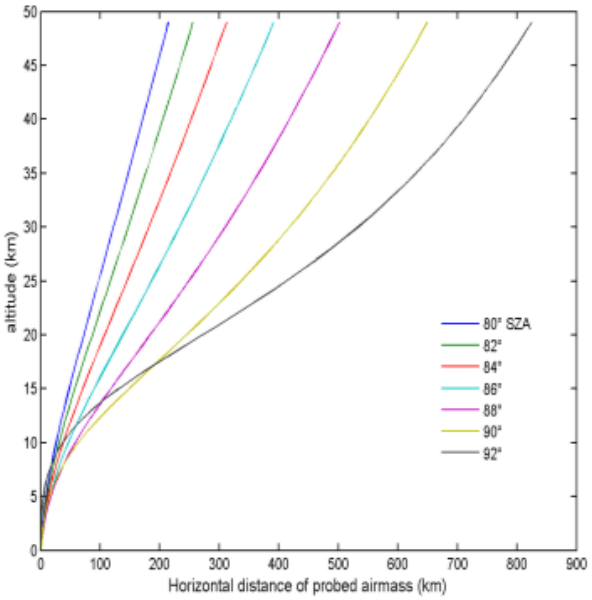

Figure 8: Average displacement of the measurement point in zenith viewing geometry for different altitudes at different solar zenith angles (M. Van Roozendael, private communication; Richter et al., 2013).

7.2 MAX-DOAS tropospheric products

Compared to zenith-sky observations, the characterisation of horizontal displacement is further complicated for MAX-DOAS tropospheric products. While in single scattering approximation the light path can still be divided into two parts, the first being determined by the solar position, the second part from the scattering point to the instrument depends on the viewing azimuth and elevation of the instrument. Also, the distance of the last scattering point from the instrument is strongly dependent on wavelength and aerosol load and profile and can only be determined from the measurements themselves using the O_4 absorption. This is illustrated in Figure 9, where 2D box air mass factors (box-AMF) are shown for two wavelengths without aerosols (left and middle) and with an AOD of 0.5 in the lowest 1 km. Without aerosol, horizontal displacements of up to 200 km are possible at 500 nm, of about 50 km at 360 nm and much less in the presence of aerosols.

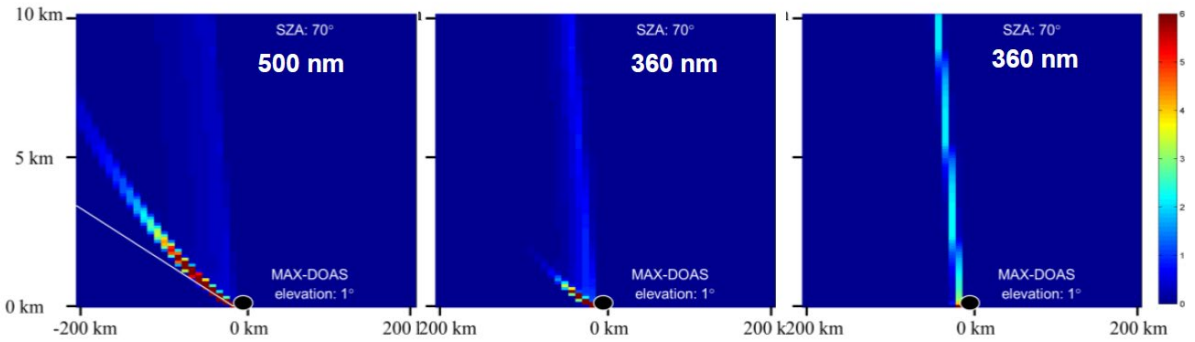

Figure 9: 2d box AMF for MAX-DOAS observations at 1° elevation and an SZA of 70°. Left: 500 nm, no aerosol. Middle: 360 nm, no aerosol. Right: 360 nm, AOD 0.5 in lowest km. All calculations have been done using a horizontal grid of 8 x 8 km² and a vertical grid of 100 m. The deviation of the line of high box-AMF from a straight line is caused by the Earth's curvature (Richter et al., 2013).

The horizontal displacement can be derived using a universal 2D polynomial function of the SZA and the relative azimuth angle (RAZI), which describes the ratio between the measured O_4 DAMF ($AM_{90°}$-$AMF_{off\text{-}axis}$) and the horizontal distance (in km), as described in Wagner and Beirle (2016). This 2D function has been determined based on RTM simulations of O_4 DAMF for different wavelength (360nm, 477nm, 577nm, and 630nm), SZA (0, 10, 20, 30, 40, 50, 60, 70, 80, 85, 88, 90°), RAZI (0, 5, 10, 20, 30, 50, 70, 90, 120, 150, 180), elevation angle (1, 2, 3, 6°), and AOD (0, 0.05, 0.1, 0.2, 0.5, 1, 2, 3) scenarios.

It should be noted that for retrievals based on elevation angles higher than 6° (e.g. 15° or 30° as often used for the geometric approximation), the effect of the atmospheric visibility is much weaker. Also, the horizontal distance, for which these observations are sensitive, is rather small: for a trace gas layer between the surface and 1km, the horizontal sensitivity range will e.g. be only between about 2 and 4 km for elevation angles of 30° and 15°, respectively. Thus in this case, the horizontal sensitivity range (D) for elevation angles (α) larger than about 10° is parameterized by the following linear relationship with the altitude (h):

$$D = h / \tan(\alpha) \tag{19}$$

8 Impact of clouds

MAX-DOAS retrievals of trace-gas and aerosol profiles and columns typically assume clear-sky conditions in forward model simulations. However, MAX-DOAS measurements, in contrast to twilight zenith-sky observations, are often strongly affected by clouds, leading to significant data quality degradation and larger uncertainties on the retrievals. This, in turn, strongly impairs the use of ground-based retrievals in the context of satellite and model validation.

Cloud-free sky conditions are ideal for the profile inversion, as under cloudy skies the atmospheric light paths are complicated, especially for rapidly changing cloud conditions. In principle, it would be possible to include clouds in the radiative transfer simulations, but usually the necessary information on cloud properties is not available (e.g. Erle et al., 1995; Wagner et al., 1998, 2002, 2004; Winterrath et al., 1999). So, it is important to identify and classify clouds and aerosols for each measurement in order to characterise the quality of the retrieval.

Cloud information derived from MAX-DOAS observations, instead of other sources like e.g. visual inspection or camera images, is very important, because it can be directly assigned to individual MAX-DOAS observations without any spatio-temporal interpolation and without requiring the installation of additional instrumentation. This is especially important for future harmonised MAX-DOAS data processing in global monitoring networks of tropospheric species.

Several cloud-screening methods using MAX-DOAS measurements have been developed recently (Wagner et al., 2014 and 2016; Gielen et al. 2014; Wang et al., 2015 and 2017; see also Richter et al., 2016), based on parameters such as the colour index and the absorption of the oxygen dimer. These cloud-screening schemes typically differentiate between a few primary sky conditions, such as: clear sky (with low/high aerosol load), continuous clouds, cloud holes, broken/scattered clouds, and secondary conditions such as thick clouds or fog.

9 Conclusions

The present ATBD gives an overview on the state-of-the-art methodologies used to retrieve profile and column products from MAX-DOAS and zenith-sky twilight observations at NDACC UV-Vis stations. The error budgets corresponding to these products are also described, as well as their vertical resolution, horizontal representativeness, and sensitivity to the presence of clouds, which are three important parameters for the quality assessment of the retrievals.

10 References

Barthia, P. K., C. G. Wellemeyer, S. L. Taylor, N. Nath, and A. Gopolan, Solar Backscatter (SBUV) Version 8 profile algorithm, Proceedings of the Quadrennial Ozone Symposium 2004, edited by C. Zerefos, pp. 295-296, Athens, Greece, ISBN, 960-630-103-6, 2004.

Barret, B., M. De Mazière, and P. Demoulin, Retrieval and characterisation of ozone profiles from solar infrared spectra at the Jungfraujoch, J. Geophys. Res., 107, doi:10.1029 / 2001JD001298, 2002.

Beirle, S., Dörner, S., Donner, S., Remmers, J., Wang, Y., and Wagner, T.: The Mainz profile algorithm (MAPA), Atmos. Meas. Tech., 12, 1785–1806, https://doi.org/10.5194/amt-12-1785-2019, 2019.

Clémer, K., M. Van Roozendael, C. Fayt, F. Hendrick, C. Hermans, G. Pinardi, R. Spurr, P. Wang, and M. De Mazière, Multiple wavelength retrieval of tropospheric aerosol optical properties from MAXDOAS measurements in Beijing, Atmos. Meas. Tech, 3, 863-878, 2010.

Eskes, H. J., and K. F. Boersma, Averaging kernels for DOAS total-column satellite retrievals, Atmos. Chem. Phys., 3, 1285–1291, 2003.

Fayt, C., De Smedt, I., Letocart, V., Merlaud, A., Pinardi, G., and Van Roozendael, M.: QDOAS Software user manual, http: //uv-vis.aeronomie.be/software/QDOAS/index.php, 2011.

Fiedler M., H. Frank, T. Gomer, M. Hausmann, K. Pfeilsticker, and U. Platt, Groundbased spectroscopic measurements of stratospheric NO_2 and OClO in arctic winter 1989/90, Geophys. Res. Lett., 20, 963-966, 1993.

Friedrich, M. M., Rivera, C., Stremme, W., Ojeda, Z., Arellano, J., Bezanilla, A., García-Reynoso, J. A., and Grutter, M.: NO_2 vertical profiles and column densities from MAX-DOAS measurements in Mexico City, Atmos. Meas. Tech., 12, 2545–2565, https://doi.org/10.5194/amt-12-2545-2019, 2019.

Frieß U., P. S. Monks, J. J. Remedios, A. Rozanov, R. Sinreich, T. Wagner, and U. Platt, MAX-DOAS O_4 measurements: A new technique to derive information on atmospheric aerosols: 2. Modeling studies, J. Geophys. Res. 111, D14203, doi:10.1029/2005JD006618, 2006.

Frieß, U., Beirle, S., Alvarado Bonilla, L., Bösch, T., Friedrich, M. M., Hendrick, F., Piters, A., Richter, A., van Roozendael, M., Rozanov, V. V., Spinei, E., Tirpitz, J.-L., Vlemmix, T., Wagner, T., and Wang, Y.: Intercomparison of MAX-DOAS vertical profile retrieval algorithms: studies using synthetic data, Atmos. Meas. Tech., 12, 2155–2181, https://doi.org/10.5194/amt-12-2155-2019, 2019.

Gielen, C., M. Van Roozendael, F. Hendrick, G. Pinardi, T. Vlemmix, V. De Bock, H. De Backer, C. Fayt, C. Hermans, D. Gillotay, and P. Wang, A simple and versatile cloud-screening method for MAX-DOAS retrievals, Atmos. Meas. Tech., 7, 3509-3527, doi:10.5194/amt-7-3509-2014, 2014.

Hendrick, F., B. Barret, M. Van Roozendael, H. Boesch, A. Butz, M. De Mazière, F. Goutail, C. Hermans, J.-C. Lambert, K. Pfeilsticker, and J.-P. Pommereau, Retrieval of nitrogen dioxide stratospheric profiles from ground-based zenith-sky UV-visible observations: Validation of the technique through correlative comparisons, Atmos. Chem. Phys., 4, 2091-2106, 2004.

Hendrick, F., M. Van Roozendael, A. Kylling, A. Petritoli, A. Rozanov, S. Sanghavi, R. Schofield, C. von Friedeburg, T. Wagner, F. Wittrock, D. Fonteyn, and M. De Mazière, Intercomparison exercise between different radiative transfer models used for the interpretation of ground-based zenith-sky and multi-axis DOAS observations, Atmos. Chem. Phys., 6, 93-108, 2006.

Hendrick, F., P.V. Johnston, K. Kreher, C. Hermans, M. De Mazière, and M. Van Roozendael, One decade trend analysis of stratospheric BrO over Harestua (60°N) and Lauder (44°S) reveals a decline, Geophys. Res. Lett., 35, L14801, doi:10.1029/2008GL034154, 2008.

Hendrick, F., A. Rozanov, P. V. Johnston, H. Bovensmann, M. De Mazière, C. Fayt, C. Hermans, K. Kreher, W. Lotz, B.-M. Sinnhuber, N. Theys, A. Thomas, J. P. Burrows, and M. Van Roozendael, Multi-year

comparison of stratospheric BrO vertical profiles retrieved from SCIAMACHY limb and ground-based UV-visible measurements, Atmos. Meas. Tech., 1, 273-285, 2009.

Hendrick, F., J.-P. Pommereau, F. Goutail, R. D. Evans, D. Ionov, A. Pazmino, E. Kyrö, G. Held, P. Eriksen, V. Dorokhov, M. Gil, and M. Van Roozendael, NDACC/SAOZ UV-visible total ozone measurements: Improved retrieval and comparison with correlative ground-based and satellite observations, Atm. Chem. Phys., 11, 5975-5995, 2011.

Hönninger, G., C. von Friedeburg, and U. Platt, Multi axis differential optical absorption spectroscopy (MAX-DOAS), Atmos. Chem. Phys., 4, 231–254, doi:10.5194/acp-4-231-2004, 2004.

Kreher, K., P. V. Johnston, S. W. Wood, and U. Platt, Ground-based measurements of tropospheric and stratospheric BrO at Arrival Heights (78°S), Antarctica, Geophys. Res. Lett., 24, 3021-3024, 1997.

Kreher, K., Van Roozendael, M., Hendrick, F., Apituley, A., Dimitropoulou, E., Frieß, U., Richter, A., Wagner, T., Abuhassan, N., Ang, L., Anguas, M., Bais, A., Benavent, N., Bösch, T., Bognar, K., Borovski, A., Bruchkouski, I., Cede, A., Chan, K. L., Donner, S., Drosoglou, T., Fayt, C., Finkenzeller, H., Garcia-Nieto, D., Gielen, C., Gómez-Martín, L., Hao, N., Herman, J. R., Hermans, C., Hoque, S., Irie, H., Jin, J., Johnston, P., Khayyam Butt, J., Khokhar, F., Koenig, T. K., Kuhn, J., Kumar, V., Lampel, J., Liu, C., Ma, J., Merlaud, A., Mishra, A. K., Müller, M., Navarro-Comas, M., Ostendorf, M., Pazmino, A., Peters, E., Pinardi, G., Pinharanda, M., Piters, A., Platt, U., Postylyakov, O., Prados-Roman, C., Puentedura, O., Querel, R., Saiz-Lopez, A., Schönhardt, A., Schreier, S. F., Seyler, A., Sinha, V., Spinei, E., Strong, K., Tack, F., Tian, X., Tiefengraber, M., Tirpitz, J.-L., van Gent, J., Volkamer, R., Vrekoussis, M., Wang, S., Wang, Z., Wenig, M., Wittrock, F., Xie, P. H., Xu, J., Yela, M., Zhang, C., and Zhao, X.: Intercomparison of NO_2, O_4, O_3 and HCHO slant column measurements by MAX-DOAS and zenith-sky UV-Visible spectrometers during the CINDI-2 campaign, Atmos. Meas. Tech. Discuss., https://doi.org/10.5194/amt-2019-157, in review, 2019.

Lambert, J.-C., J. Granville, M. Van Roozendael, A. Sarkissian, F. Goutail, J.-F. Müller, J.-P. Pommereau, and J.M. Russell III, A climatology of NO2 profile for improved Air Mass Factors for ground-based vertical column measurements, in Stratospheric Ozone 1999, N.R.P. Harris, M. Guirlet, and G.T. Amanatidis (Eds.), Air Pollution Research Report 73 (CEC DG XII), pp. 703-706, 1999.

Lambert, J.-C., J. Granville, M. Van Roozendael, J.-F. Müller, F. Goutail, J.-P. Pommereau, A. Sarkissian, P. V. Johnston, and J. M. Russell III, Global Behaviour of Atmospheric NO2 as Derived from the Integrated Use of Satellite, Ground-based Network and Balloon Observations, in Atmospheric Ozone - 19th Quad. Ozone Symp., Sapporo, Japan, 2000, Ed. by NASDA, pp. 201-202, 2000.

Li, X., T. Brauers, M.Shao, R. M. Garland, T. Wagner, T. Deutschmann, and A. Wahner, MAX-DOAS measurements in southern China: retrieval of aerosol extinctions and validation using ground-based in-situ data, Atmos. Chem. Phys., 10, 2079–2089, doi:10.5194/acp-10-2079-2010, 2010.

Mayer, B., and A. Kylling, Technical note: The libRadtran software package for radiative transfer calculations - description and examples of use, Atmos. Chem. Phys., 5, 1855-1877, 2005.

McKenzie, R., P. V. Johnston, C. T. McElroy, J. B. Kerr, and S. Solomon, Altitude distributions of stratospheric constituents from ground-based measurements at twilight, J. Geophys. Res., 96, 15499-15511, 1991.

Platt, U., and J. Stuz, Differential Optical Absorption Spectroscopy (DOAS), Principles and Applications, ISBN 978-3-540-21193-8, Springer, Berlin-Heidelberg, 2008.

Pommereau, J. P., and F. Goutail, O_3 and NO_2 ground-based measurements by visible spectrometry during Arctic winter and spring 1988, Geophys. Res. Lett., 15, 891-894, 1988.

Preston, K. E., R. L. Jones, and H. K. Roscoe, Retrieval of NO_2 vertical profiles from ground-based UV-visible measurements: Method and validation, J. Geophys. Res., 102 (D15), 19,089-19,097, 1997.

Richter, A., M. Eisinger, A. Ladstätter Weißenmayer, F. Wittrock, and J. P. Burrows, DOAS zenith-sky observations: 2. Seasonal variations of BrO over Bremen (53°N) 1994-1995, J. Atmos. Chem., 32, 83-99, 1999.

Richter, A., S. Godin, L. Gomez, F. Hendrick, K. Hocke, B. Langerock, M. Van Roozendael, T. Wagner, NORS Deliverable D4.4 'Spatial Representativeness of NORS observations', November 2013 – See http://nors.aeronomie.be/projectdir/PDF/D4.4_NORS_SR.pdf.

Richter, A., A. Bais, B. Dils, C. Gielen, F. Hendrick, G. Pinardi, E. Peters, A. Piters, J. Remmers, T. Wagner, S. Wang, Y. Wang, QA_4ECV Deliverable D3.9 'Quality indicators on uncertainties and representativity of atmospheric reference data', November 2016 – See http://www.qa4ecv.eu/sites/default/files/D3.9.pdf

Rodgers, C. D., Inverse Methods for Atmospheric Sounding, Theory and Practice. World Scientific Publishing, Singapore-NewJersey-London-Hong Kong, 2000.

Roscoe, H. K., Johnston, P. V, Van Roozendael, M., Richter, A., Sarkissian, A., Roscoe, J., Preston, K. E., Lambert, J.-C., Hermans, C., Decuyper, W., Dzienus, S., Winterrath, T., Burrows, J. B., Goutail, F., Pommereau, J.-P., D'Almeida, E., Hottier, J., Coureul, C., Didier, R., Pundt, I., Bartlett, L. M., McElroy, C. T., Kerr, J. E., Elokhov, A., Giovanelli, G., Ravegnani, F., Premuda, M., Kostadinov, I., Erle, F., Wagner, T., Pfeilsticker, K., Kenntner, M., Marquard, L. C., Gil, M., Puentedura, O., Yela, M., Arlander, D. W., Kastad Hoiskar, B. A., Tellefsen, C. W., Karlsen Tornkvist, K., Heese, B., Jones, R. L., Aliwell, S. R., Freshwater, R. A., Slant Column Measurements of O_3 and NO_2 During the NDSC Intercomparison of Zenith-Sky UV-Visible Spectrometers in June 1996. J. Atmos. Chem., 32, 281–314, 1999.

Roscoe, H. K., M. Van Roozendael, C. Fayt, A. du Piesanie, N. Abuhassan, C. Adams, M. Akrami, A. Cede, J. Chong, K. Clemer, U. Frieß, M. Gil Ojeda, F. Goutail, R. Graves, A. Griesfeller, K. Grossmann, G. Hemerijckx, F. Hendrick, J. Herman, C. Hermans , H. Irie, Y. Kanaya, K. Kreher, P. Johnston, R. Leigh, A. Merlaud, G. H. Mount, M. Navarro, H. Oetjen, A. Pazmino, M. Perez-Camacho, E. Peters, G. Pinardi, O. Puentedura, A. Richter, A. Schönhardt, R. Shaiganfar, E. Spinei, K. Strong, H. Takashima, T. Vlemmix, M. Vrekoussis, T. Wagner, F. Wittrock, M. Yela, S.Yilmaz, F. Boersma, J. Hains, M. Kroon, and A. Piters, Intercomparison of slant column measurements of NO_2 and O_4 by MAX-DOAS and zenith-sky UV and visible spectrometers, Atmos. Meas. Tech., 3, 1629-1646, 2010.

Schofield, R., K. Kreher, B. J. Connor, P. V. Johnston, A. Thomas, D. Shooter, M. P. Chipperfield, C. D. Rodgers, and G. H. Mount, Retrieved tropospheric and stratospheric BrO columns over Lauder, New Zealand, J. Geophys. Res., 109, D14304, doi:10.1029/2003JD004463, 2004.

Solomon, S., R. W. Sanders, M. A. Carroll, and A. L. Schmeltekopf, Visible and near-ultraviolet spectroscopy at McMurdo station, Antarctica, 5. Diurnal variation of OClO and BrO, J. Geophys. Res., 94, 11393-11403, 1989.

Struthers, H., K. Kreher, J. Austin, R. Schofield, G. Bodeker, P. Johnston, H. Shiona, and A. Thomas, Past and future simulations of NO_2 from a coupled chemistry-climate model in comparison with observations, Atmos. Chem. Phys, 4, 2227-2239, 2004.

Tirpitz, J.-L., Frieß, U., Hendrick, F., Alberti, C., Allaart, M., Apituley, A., Bais, A., Beirle, S., Berkhout, S., Bognar, K., Bösch, T., Bruchkouski, I., Cede, A., Chan, K. L., den Hoed, M., Donner, S., Drosoglou, T., Fayt, C., Friedrich, M. M., Frumau, A., Gast, L., Gielen, C., Gomez-Martín, L., Hao, N., Hensen, A., Henzing, B., Hermans, C., Jin, J., Kreher, K., Kuhn, J., Lampel, J., Li, A., Liu, C., Liu, H., Ma, J., Merlaud, A., Peters, E., Pinardi, G., Piters, A., Platt, U., Puentedura, O., Richter, A., Schmitt, S., Spinei, E., Stein Zweers, D., Strong, K., Swart, D., Tack, F., Tiefengraber, M., van der Hoff, R., van Roozendael, M., Vlemmix, T., Vonk, J., Wagner, T., Wang, Y., Wang, Z., Wenig, M., Wiegner, M., Wittrock, F., Xie, P., Xing, C., Xu, J., Yela, M., Zhang, C., and Zhao, X.: Intercomparison of MAX-DOAS vertical profile retrieval algorithms: studies on field data from the CINDI-2 campaign, Atmos. Meas. Tech. Discuss., https://doi.org/10.5194/amt-2019-456, in review, 2020.

Vandaele, A. C., C. Fayt, F. Hendrick, C. Hermans, F. Humbled, M. Van Roozendael, M. Gil, M. Navarro, O. Puentedura, M. Yela, G. Braathen, K. Stebel, K.Tørnkvist, P. Johnston, K. Kreher, F. Goutail, A. Mieville, J.-P. Pommereau, S. Khaikine, A. Richter, H. Oetjen, F. Wittrock, S. Bugarski, U. Frieß, K. Pfeilsticker, R. Sinreich, T. Wagner, G. Corlett, and R. Leigh, An intercomparison campaign of ground-based UV-Visible measurements of NO_2, BrO, and OClO slant columns. Methods of analysis and results for NO_2, J. Geophys. Res., 110, D08305, doi:10.1029/2004JD005423, 2005.

Van Roozendael, M., M. De Mazière, and P. C. Simon, Ground-based visible measurements at the Jungfraujoch station since 1990, J. Quant. Spectrosc. Radiat. Transfer, 52 (3/4), 231-240, 1994.

Van Roozendael, M., P. Peters, H. K. Roscoe, H. De Backer, A. E. Jones, L. Bartlett, G. Vaughan, F. Goutail, J.-P. Pommereau, E. Kyrö, C. Wahlstrom, G. Braathen, and P. C. Simon, Validation of ground-based visible measurements of total ozone by comparison with Dobson and Brewer spectrophotometers, J. Atm. Chem., 29, 55-83, 1998.

Vlemmix, T., Piters, A. J. M., Stammes, P., Wang, P., and Levelt, P. F.: Retrieval of tropospheric NO_2 using the MAX-DOAS method combined with relative intensity measurements for aerosol correction, Atmos. Meas. Tech., 3, 1287–1305, https://doi.org/10.5194/amt-3-1287-2010, 2010.

Vlemmix, T., A. J. M.Piters, A. J. C. Berkhout, L. F. L. Gast, P. Wang, and P. F. Levelt, Ability of the MAX-DOAS method to derive profile information for NO_2: can the boundary layer and free troposphere be separated?, Atmos. Meas. Tech., 4, 2659–2684, doi:10.5194/amt-4-2659-2011, 2011.

Vlemmix, T., F. Hendrick, G. Pinardi, I. De Smedt, C. Fayt, C. Hermans, A. Piters, P. Levelt, and M. Van Roozendael, MAX-DOAS observations of aerosols, formaldehyde and nitrogen dioxide in the Beijing area: comparison of two profile retrieval approaches, Atmos. Meas. Tech., 8, 941-963, 2015.

Wagner, T., F. Erie, L. Marquard, C. Otten, K. Pfeilsticker, T. Senne, J. Stutz, and U. Platt, Cloudy sky optical paths as derived from differential optical absorption spectroscopy observations, J. Geophys. Res., 103, 25307, doi:10.1029/98JD01021, 1998.

Wagner, T., C. von Friedeburg, M. Wenig, C. Otten, and U. Platt, UV/vis observations of atmospheric O_4 absorptions using direct moon light and zenith scattered sunlight under clear and cloudy sky conditions, J. Geophys. Res., 107, D204424, doi:10.1029/2001JD001026, 2002.

Wagner T., B. Dix, C. von Friedeburg, U. Frieß, S. Sanghavi, R. Sinreich, and U. Platt, MAX-DOAS O_4 measurements: A new technique to derive information on atmospheric aerosols – Principles and information content, J. Geophys. Res. 109, D22205, doi:10.1029/2004JD004904, 2004.

Wagner, T., J. P. Burrows, T. Deutschmann, B. Dix, C. von Friedeburg, U. Frieß, F. Hendrick, K.-P. Heue, H. Irie, H. Iwabuchi, Y. Kanaya, J. Keller, C. A. Mc Linden, H. Oetjen, E. Palazzi, A. Petritoli, U. Platt, O. Postylyakov, J. Pukite, A. Richter, M. Van Roozendael, A. Rozanov, R. Sinreich, S. Sanghavi, S., and Wittrock, F. : Comparison of box-air-mass-factors and radiances for multiple-axis differential optical absorption spectroscopy (MAX-DOAS) geometries calculated from different UV/visible radiative transfer models, Atmos. Chem. Phys., 7, 1809-1833, 2007.

Wagner, T., S. Beirle, T. Brauers, T. Deutschmann, U. Frieß, C. Hak, J. D. Halla, K. P. Heue, W. Junkermann, X. Li, U. Platt, and I. Pundt-Gruber, Inversion of tropospheric profiles of aerosol extinction and HCHO and NO_2 mixing ratios from MAX-DOAS observations in Milano during the summer of 2003 and comparison with independent data sets, Atmos. Meas. Tech., 4, 2685-2715, doi:10.5194/amt-4-2685-2011, 2011.

Wagner, T., A. Apituley, S. Beirle, S. Dörner, U. Frieß, J. Remmers, and R. Shaiganfar, Cloud detection and classification based on MAX-DOAS observations, Atmos. Meas. Tech., 7, 1289-1320, doi:10.5194/amt-7-1289-2014, 2014.

Wagner, T., and S. Beirle, QA$_4$ECV Technical Note: Estimation of the horizontal sensitivity range from MAX-DOAS O_4 observations, April 2016.

Wagner, T., S. Beirle, J. Remmers, R. Shaiganfar, and Y. Wang, Absolute calibration of the colour index and O_4 absorption derived from Multi AXis (MAX-)DOAS measurements and their application to a standardised cloud classification algorithm, Atmos. Meas. Tech., 9, 4803-4823, doi:10.5194/amt-9-4803-2016, 2016.

Wang, Y., M. Penning de Vries, P. Xie, S. Beirle, S. Dörner, J. Remmers, A. Li, and T. Wagner, Cloud and aerosol classification for 2.5 years of MAX-DOAS observations in Wuxi (China) and comparison to independent data sets, Atmos. Meas. Tech., 8, 5133-5156, doi:10.5194/amt-8-5133-2015, 2015.

Wang, Y., J. Lampel, P. Xie, S. beirle, A. Li, D. Wu, and T. Wagner, Ground-based MAX-DOAS observations of tropospheric aerosols, NO_2, SO_2, and HCHO in Wuxi, China, from 2011 to 2014, 17, 2189–2215, 2017, doi:10.5194/acp-17-2189-2017.

Winterrath, T., T. P. Koruso, A. Richter, and J. P. Burrows, Enhanced O_3 and NO_2 in thunderstorm clouds: convection or production, Geophys. Res. Lett., 26, 1291-1294, doi:10.1029/1999GL900243, 1999.